Available online at www.sciencedirect.com
ScienceDirect
Surface Science 601 (2007) 30–43
SURFACE SCIENCE
www.elsevier.com/locate/susc

In situ XPS investigation of Pt(Sn)/Mg(Al)O catalysts during ethane dehydrogenation experiments

Anastasia Virnovskaia [a], Sissel Jørgensen [a], Jasmina Hafizovic [a], Øystein Prytz [a], Evgueni Kleimenov [b,1], Michael Hävecker [b], Hendrik Bluhm [b,2], Axel Knop-Gericke [b], Robert Schlögl [b], Unni Olsbye [a,*]

[a] *Centre for Materials Science and Nanotechnology, Department of Chemistry, University of Oslo, P.O. Box 1033 Blindern, N-0315 Oslo, Norway*
[b] *Department of Inorganic Chemistry, Fritz-Haber-Institut der Max-Planck-Gesellschaft, Faradayweg 4-6, 14195 Berlin, Germany*

Received 13 June 2006; accepted for publication 1 September 2006
Available online 25 September 2006

Abstract

Calcined hydrotalcite with or without added metal (Mg(Al)O, Pt/Mg(Al)O and Pt,Sn/Mg(Al)O) have been investigated with *in situ* X-ray photoelectron spectroscopy (XPS) during ethane dehydrogenation experiments. The temperature in the analysis chamber was 450 °C and the gas pressure was in the range 0.3–1 mbar. Depth profiling of calcined hydrotalcite and platinum catalysts under reaction, oxidation and in hydrogen–water mixture was performed by varying the photon energy, covering an analysis depth of 10–21 Å. It was observed that the Mg/Al ratio in the Mg(Al)O crystallites does not vary significantly in the analysis depth range studied. This result indicates that Mg and Al are homogeneously distributed in the Mg(Al)O crystallites. Catalytic tests have shown that the initial activity of a Pt,Sn/Mg(Al)O catalyst increases during an activation period consisting of several cycles of reduction–dehydrogenation–oxidation. The Sn/Mg ratio in a Pt,Sn/Mg(Al)O catalyst was followed during several such cycles, and was found to increase during the activation period, probably due to a process where tin spreads over the carrier material and covers an increasing fraction of the Mg(Al)O surface. The results further indicate that spreading of tin occurs under reduction conditions.

A $PtSn_2$ alloy was studied separately. The surface of the alloy was enriched in Sn during reduction and reaction conditions at 450 °C. Binding energies were determined and indicated that Sn on the particle surface is predominantly in an oxidised state under reaction conditions, while Pt and a fraction of Sn is present as a reduced Pt–Sn alloy.

Keywords: X-ray photoelectron spectroscopy; Catalysis; Platinum; Tin; Alkanes; Alkenes

1. Introduction

Light alkenes are important base chemicals for the chemical industry. Catalytic dehydrogenation of light alkanes is believed to be a potentially important route to selective production of high purity alkenes. Two classes of catalysts are used in commercial dehydrogenation processes, supported platinum–tin catalysts and chromium oxide supported on alumina [1]. The alkane dehydrogenation reaction is strongly endothermic. In Cr-based processes, heat is supplied by burning off coke deposits from the catalyst in either a fixed bed rector with alternate feed (Catofin) or in a continuously regenerated fluid bed reactor (FBD-4). In Pt-based processes, heat is supplied by external heating of either a tubular fixed bed (STAR) or an adiabatic moving-bed reactor (Oleflex) [1]. Pt-based catalysts have several advantages compared to Cr-based catalysts: First, they may be used in steam-containing atmospheres, such as under autothermal dehydrogenation conditions

* Corresponding author. Tel.: +47 22855456; fax: +47 22855441.
E-mail address: unni.olsbye@kjemi.uio.no (U. Olsbye).
[1] Present address: Physical Chemistry Laboratory, ETH Hönggerberg – HCI E 209, Wolfgang-Pauli-Strasse 10, CH-8093 Zürich, Switzerland.
[2] Present address: Lawrence Berkeley National Laboratory, Chemical Sciences Division, Berkeley, CA 94720, USA.

0039-6028/$ - see front matter © 2006 Elsevier B.V. All rights reserved.
doi:10.1016/j.susc.2006.09.002

[2,3]. Second, they are fairly stable even at temperatures $\geqslant 600$ °C, which are necessary to overcome the unfavourable Gibbs free energy of the ethane dehydrogenation reaction [3,4]. In this paper we study Pt(Sn)/Mg(Al)O ethane dehydrogenation catalysts.

Hydrotalcites and hydrotalcite-like materials, generally denoted

$$M_x^{2+}M_2^{3+}(OH^-)_{2(x+2)}(CO_3^{2-})\cdot yH_2O,$$

with M^{2+} and M^{3+} representing bi- and trivalent metal cations, respectively, and x is typically 6–10, are basic materials with many known applications [5]. After calcination at 400 °C or higher, the layered hydrotalcite structure collapses and a metastable mixed oxide phase, $M^{2+}(M^{3+})O$, is formed. After prolonged use or calcination at higher temperatures, segregation into the thermodynamically stable oxide phases, $M^{2+}M_2^{3+}O_4$ and $M^{2+}O$, occurs [6].

Mg(Al)O, prepared via the corresponding hydrotalcite phase, possesses excellent properties as support material for metal-based catalysts [5,7–10]. The support material is particularly suited for applications in an intermediate temperature range ($\leqslant 600$ °C), where it has been shown to maintain a high surface area (above 100 m^2/g) even after 14 days in a steam-rich atmosphere [11]. Propane dehydrogenation to propene is one reaction for which the intermediate temperature range is particularly suited, and Pt,Sn/Mg(Al)O has been shown to possess superior activity and stability for this reaction compared to conventional $Pt,Sn/Al_2O_3$ catalysts [7].

The aim of the present study is to characterise Pt,Sn/Mg(Al)O during use as an ethane dehydrogenation catalyst, in order to improve the fundamental understanding of this complex catalytic system. *In situ* X-ray photoelectron spectroscopy (XPS) was chosen as the main characterisation method. Two features were chosen for further elucidation:

1. Several literature reports have concluded that the surface of the Mg(Al)O mixed oxide phase is enriched in aluminium [12–14]. Such enrichment is intuitively appealing, and has great impact on e.g. modelling of catalytic reaction cycles which involve the support surface. One example is dry reforming of propane to synthesis gas, where the Mg(Al)O surface has been shown to activate CO_2 [10]. The unique possibility of tuning the photon energy in synchrotron-based XPS makes it suitable for depth profiling of irregular powder surfaces such as the Mg(Al)O multicrystallites under reaction conditions [15]. In this work, photon energy variation was used to obtain unprecedented insight into the distribution of Mg and Al in Mg(Al)O.
2. Pt–Sn catalysts are subject of numerous articles in the open literature. Most studies report advantageous effects of promoting Pt catalysts with Sn: Tin promotion improves catalytic activity, dehydrogenation selectivity, prevents Pt sintering, and decreases deactivation due to coke formation (see e.g. [4,16–23] and references therein). There is controversy in literature about the oxidation state of Sn, and an effect of the support material, Pt-to-Sn ratio and preparation method is suggested [17,19,21,24].

Only a few reports in the open literature have been devoted to the system under study; Pt,Sn/Mg(Al)O [4,7,15,16,25,26]. The activity pattern of a proprietary 0.25wt%Pt,0.5wt%Sn/Mg(Al)O catalyst is quite peculiar, in that the initial activity increases during repeated dehydrogenation–regeneration cycles [15]. This activity increase makes the system particularly suited for elucidating information on the active state of the catalyst, using *in situ* methods. Previous studies using *ex situ* TEM indicated that the metal particles are enriched in Pt during reduction, most particles containing 60–90 wt% Pt [4,16]. CO adsorption measurements suggested an electronic interaction between the support material and the metal particles, leading to less CO adsorption on Pt,Sn/Mg(Al)O than expected from activity measurements of Pt,Sn/Mg(Al)O and $Pt,Sn/Al_2O_3$ [15,16]. In the present study, *in situ* XPS was used to obtain real-time information about the distribution of Sn in the catalyst, by following the Sn/Mg ratio with time on stream during repeated dehydrogenation–regeneration cycles. In order to enhance the detectability of Sn, a catalyst enriched in Pt and Sn (compared to the proprietary catalyst) was used for these measurements. Catalytic testing confirmed that the model catalyst follows the same activation pattern as the proprietary catalyst (vide ultra). The present study is complementary to the previous TEM work: While metallic Sn is almost indistinguishable from the Mg(Al)O support in TEM, no overlap between Sn peaks and the peaks of the support material exist for the XPS technique. On the other hand, while Pt is easily detected by TEM, in XPS there is an overlap between the main Pt peak (4f) and Al 2p, rendering it difficult to study Pt on Mg(Al)O supports by XPS. In order to overcome the problem with overlap of Pt 4f and Al 2p peaks in XPS, supplementary information about Pt,Sn surface ratios and Pt,Sn oxidation states during a reduction–dehydrogenation cycle was obtained by performing *in situ* XPS studies of a pure $PtSn_2$ alloy.

To our knowledge, this is the first report where a supported Pt,Sn catalyst has been followed by *in situ* methods throughout several test-regeneration cycles.

2. Experimental

2.1. Sample preparation and characterisation

The carrier material Mg(Al)O with a Mg/Al ratio of 4.8 was synthesised via the corresponding hydrotalcite phase, using a standard co-precipitation method as described in Ref. [15]. After drying, the obtained $Mg_{9.6}Al_2(OH)_{19.2}$-$CO_3\cdot xH_2O$ phase was calcined at 600 °C in air for approximately 15 h to yield the final Mg(Al)O phase.

Pt/Mg(Al)O catalysts were prepared by impregnation of Pt onto the uncalcined carrier material from an excess solution of hexachloroplatinic acid ($H_2PtCl_6 \cdot 4H_2O$) in water (sample Pt-1) or ethanol (sample Pt-2) under a He atmosphere. $H_2PtCl_6 \cdot 4H_2O$ (0.0776 g) was dissolved in ion exchanged water or 96% ethanol (30 mL). The hydrotalcite (1.00 g) was added to the salt solution under stirring. After 30 min, the slurry was filtered and the solid material washed with the solvent three times (approximately 30 mL), dried at 100 °C and finally calcined in air at 600 °C for approximately 15 h. The Pt content of the Pt/Mg(Al)O catalysts was determined by ICP analysis. The numbers given in the text refer to the calcined sample.

The active metals in Pt,Sn/Mg(Al)O were deposited onto the uncalcined hydrotalcite (HTC) by impregnation from aqueous solution as described in Ref. [15]. The sample was calcined at 800 °C in air for 5 h. Impregnation of an uncalcined HTC was chosen because previous work has indicated that this method yields a more stable dehydrogenation catalyst than impregnation of a precalcined HTC [15]. Previous studies further showed that by this preparation method, Pt(Sn) complexes are deposited by physisorption at protonated sites on the carrier material. After calcination, CO_2 adsorption, followed by temperature-programmed desorption (TPD) experiments, showed that the final metal clusters cover the most basic sites of the support material, i.e., steps and corners [16,27]. The Pt(Sn) clusters are likely to be distributed at step and corner sites at the outer surface as well as in the catalyst pores. However, since the XPS analysis depth is typically below 20 Å, i.e., less than one support crystallite diameter (vide infra), while the XPS signal is collected from a surface of 100×800 μm, the XPS results reported below are clearly dominated by metal clusters at the outer surface.

$PtSn_2$ alloy was prepared by weighing in the appropriate amounts of pure Pt and Sn metal, transferring the materials to a quartz vessel under inert atmosphere, then sealing and heating to 730 °C, maintaining this temperature for one week. The quartz vessel was then opened under an inert atmosphere, and the Pt–Sn material was crushed and returned to the vessel, which was sealed and left for one more week at 730 °C. The alloy was stored in the sealed quartz vessel until opening it for the XPS analysis. The phase purity of the alloy was confirmed by XRD analysis.

The calcined hydrotalcite-based samples were characterised by using transmission electron microscopy (TEM) and Brunauer, Emmett and Teller (BET) surface area measurements. A partially reconstructed (due to prolonged storage in air) sample was characterised by temperature resolved X-ray diffraction (XRD). All characterisation was performed on powdered samples.

The temperature-programmed X-ray diffraction analyses were recorded with a Siemens D500 diffractometer using Cu Kα radiation. The instrument was equipped with β-filter and Scintallator counter. The sample was heated from 25 to 450 °C in 25 °C steps in air using a Bühler furnace. The BET surface areas of the samples were determined by N_2 adsorption using a Monosorb instrument from Quantachrome. Samples for transmission electron microscopy were prepared by crushing in ethanol in an agate mortar, and subsequently deposited on a carbon film suspended on a copper mesh. The samples were then studied in a field emission JEOL 2010F TEM operated at 200 kV.

2.2. In situ X-ray photoelectron spectroscopy

In situ X-ray photoelectron spectroscopy was conducted in a constant gas flow, at temperatures up to 450 °C and at total pressures in the sample cell up to 1 mbar. A detailed description of the experimental conditions is given in Table 1. Before switching the gas atmosphere during *in situ* XPS measurements, the sample chamber was evacuated to the base pressure of 2×10^{-8} mbar before a different gas mixture was let in. The gas effluent was monitored by an on-line Mass Spectrometer (Pfeiffer Prisma). The powder samples were crushed in a mortar and mounted from suspension in ethanol on a stainless steel sample holder. This mounting procedure was chosen in order to reduce charging of the powder during the XPS measurements. The $PtSn_2$ alloy was mounted in one piece between two parts of a stainless steel sample holder.

The experiments were performed at beamline UE56/2-PGM2 at the synchrotron source BESSY-II in Berlin [28]. The *in situ* XPS system is a modified standard XPS spectrometer [29] which operates analogously to the setup described in [30]. The Al 2p, Mg 2p, Sn 3d, Sn 4d, Pt 4f, C 1s and Fermi edge (FE) regions were recorded in our experiments. The incident photon energy was varied in the range 340–1040 eV, and full range of kinetic energy was used for survey scans. Detailed scans covering narrower regions were used to obtain detailed information about e.g. the Fermi level and the oxidation state of each element. During depth profiling analysis, the photon energy was varied in a way that provided similar kinetic energy of the photoelectrons for each element at each depth. In addition to a uniform information depth, equal kinetic energy of the photoelectrons provided a constant analyzer transmission function contribution and a constant gas phase scattering contribution. The inelastic mean free path (IMFP) was calculated using the NIST software [31] based on Ref. [32] for the supported samples, and based on a predictive formula (TPP-2M) from Ref. [33] for the

Table 1
Temperatures, gases and pressures in the reaction chamber

Conditions label	*T* [°C]	Gas mixture	Gas ratio	Total pressure [mbar]
UHV-RT	Ambient	UHV		2×10^{-8}
H_2-RT	Ambient	H_2		1
H_2	450	H_2		1
Rx	450	H_2O:H_2:C_2H_6	1:1.5:7.5	0.3
O_2	450	O_2		0.3
$H_2 + H_2O$	450	H_2:H_2O	1:1.5	0.25

alloy. The IMFP in MgO was used to estimate the IMFP in the Mg(Al)O samples since calcined Mg(Al)O has an MgO-like structure. The difference in the calculated IMFP values of MgO and Al_2O_3 is below 10%, which is assumed to be within the uncertainty of the calculated IMFP. Also, the IMFP in the Mg(Al)O could be expected to be somewhat higher than the IMFP in MgO because of more insulating nature of Mg(Al)O. Table 2 shows core levels and photon energies used in the experiments, as well as the calculated analysis depth (i.e., inelastic mean free path) for each element.

2.3. Peak analysis

The peak profile of the Sn peaks in the $PtSn_2$ alloy, and changes in the Sn peak shapes during measurements, suggested the presence of two oxidation states of Sn in the alloy. The $Sn\,3d_{5/2}$ peak and Sn 4d doublet were therefore deconvoluted by Gaussian–Lorentzian curves to fit two oxidation states. The fitting parameters are shown in Table 3. The Sn 4d doublet was fitted with four curves, i.e., a doublet was assigned for each of the two oxidation states. The theoretical intensity ratio of 1.5 between the 3/2 and 5/2 components of the same chemical state was used. The full width at half maximum (FWHM) of the $Sn\,4d_{3/2}$ and $4d_{5/2}$ components was set to be equal, as observed by Pollak et al. [34], and the separation of 1 eV was used [35,36].

It should be noted that the experimental intensity ratio of the components in the spin–orbit doublet can deviate from the theoretical value, and a value of 1.3 has been reported for the Sn 4d doublet [34]. A deviation in intensity ratio of the peaks in the spin–orbit doublet used in the deconvolution procedure would mean that the absolute ratio of the chemical states would not be entirely correct, but the relative changes would be valid. In our case, if the intensity ratio used in curve fitting is higher than the ratio present in the measurements, a systematic error towards higher amounts of the chemical state with lower binding energy will be present. We chose to use the theoretical value in this work because the primary goal is to follow the changes in the oxidation states of the metals, not to determine absolute ratios.

Since the binding energy and the peak shape of the Pt peaks (4d and 4f) remained unchanged during measurements, indicating unchanged oxidation state of Pt, no deconvolution of Pt-peaks was performed.

The Al 2p peak of the support in the Pt-containing catalysts overlapped with the Pt 4f doublet. The spectra were deconvoluted using peak fitting with three Gaussian curves of equal FWHM. For each photon energy, the FWHM of the Al 2p peak in the Pt-containing samples was estimated from the width of the Al 2p peak in the carrier material. The theoretical intensity ratio of 1.33, and peak separation of 3.3 eV [35] was used for the spin–orbit doublet of Pt 4f.

2.4. Catalytic testing

The *in situ* XPS cell has a large inner volume compared to the catalytic sample amount, and it is difficult to make quantitative measurements of reactant conversion. Therefore, additional catalytic tests of the Pt,Sn/Mg(Al)O material were carried out in an ordinary test rig under

Table 2
Core levels and photon energies used in the experiments, as well as the calculated analysis depth (i.e., inelastic mean free path) for each element

Sample scanned	Element	Core level	*hv* [eV]	Kinetic energy [eV]	IMFP [Å]
Mg(Al)O	Al	2p	414	340	10
Pt/Mg(Al)O-1			644	570	14
Pt/Mg(Al)O-2			814	740	17
			1014	940	21
	Mg	2p	390	340	10
			620	570	14
			790	740	17
			990	940	21
Pt,Sn/Mg(Al)O	Sn	3d	820	334	10
			1040	554	14
	Al	2p	414	340	10
			634	560	14
	Mg	2p	390	340	10
			610	560	14
$PtSn_2$ alloy	Sn	3d	820	334	8
		4d	340	314	8
			820	794	15
	Pt	4f	390	318	8
			820	748	15
	Pt, Sn	Fermi edge (valence electrons)	390	<5	>30[a]
			820	<5	>30

[a] According to the universal curve presented in Ref. [62].

Table 3
Fitting parameters of the Sn peaks in $PtSn_2$ alloy

Peak identity	Binding energy of the fitted peaks [eV]	Fitted peak profile	% Lorentzian	FWHM [eV]	Separation of the fitted peaks [eV]
$Sn\,3d_{5/2}$	486.5 ± 0.1	Gaussian–Lorentzian product form (GL)	50	1.5 ± 0.2	1.2 ± 0.1
	485.35 ± 0.05	GL	90	0.8 ± 0.1	
$Sn\,4d_{5/2}$	25.9 ± 0.1	GL	50	1.35 ± 0.10 1.9 ± 0.1[a]	1.4 ± 0.1
	24.5 ± 0.2	GL	50	0.8 ± 0.2	

[a] Higher FWHM was used for the peaks measured at room temperature because of observed decrease of peak width upon heating. The peak broadening at room temperature can be due to charging of carbon and other impurities, as well as of the oxide layer on the surface of the alloy.

conditions as close as possible to those used in the *in situ* XPS cell. A tubular fixed bed quartz reactor with inner diameter 16 mm was heated by a tubular furnace. The temperature in the catalyst bed was measured by a thermocouple contained in a quartz thermocouple well (outer diameter 3 mm) which was centred axially inside the reactor. Prior to catalytic testing the catalyst was pressed (5 tons) to tablets, then crushed and sieved. The sieved catalyst particles (0.6 g, 0.125–0.25 mm particle size, diluted with 2.4 g quartz particles of the same size) was tested at atmospheric total pressure at 450 °C. The activation procedure consisted of cycles of 30 min reduction (3 mL/min H_2, 450 °C), 2 h ethane dehydrogenation (10.0% C_2H_6, 1.6% H_2, 6.8% CO_2, 5.9% N_2 and 75.7% Ar, totally 126 mL/min) and 4 h regeneration by O_2 diluted with inert. The oxygen content was initially 4 mol% and was increased in four steps up to 24 mol%. The reactor effluent was analysed in a HP Quad Micro-GC with 10 m Molsieve-5 Å, PoraPlot-U and AluminaPlot columns and Thermal Conductivity detectors.

3. Results and discussion

3.1. Sample characterisation

Table 4 shows the Mg/Al ratio, Pt and Sn content, and BET surface areas for the four samples studied. All samples are prepared from the same support material. The crystallite size of the support material was estimated from the BET areas, assuming cubic particles, and is also shown in Table 4. TEM images were obtained for all samples, and two representative images are shown in Fig. 1. Thorough investigation of the images indicates a Mg(Al)O crystallite diameter of 50–150 Å, in good agreement with the particle sizes estimated from BET areas.

It is well known that during storage in humid air, the Mg(Al)O phase may be partially reconverted to the corresponding hydrotalcite phase (the so-called "memory effect") [5,37]. Although the samples used in this study were calcined at 600 °C shortly before the *in situ* XPS measurements, a possible partial reformation of a hydrotalcite phase before the measurements could not be completely ruled out. A calcined Mg(Al)O support material, which had been stored in air for several month, was investigated by *in situ* X-ray diffraction during heating to 450 °C (Fig. 2). The material showed the typical XRD pattern of a hydrotalcite phase together with mixed oxide phase at room temperature [5], and transition to the Mg(Al)O phase is concluded at 400 °C. This result clearly indicates that possible hydrotalcite traces in the sample before measurements would be reconverted to Mg(Al)O during heating to the conditions used during the *in situ* XPS measurements at 450 °C, i.e., the measurements reported here were performed on a pure Mg(Al)O phase.

Table 4
The Mg/Al ratio, Pt and Sn content, BET surface areas and calculated crystallite sizes for the five samples studied

Sample label	Sample	Mg/Al [atomic ratio]	wt% Pt	wt% Sn	BET surface area [m^2/g]	Crystallite size[a] [Å]
HT	Mg(Al)O	4.8	0	0	143	117
Pt-1	Pt/Mg(Al)O-1	4.8	2.9	0	–[b]	–
Pt-2	Pt/Mg(Al)O-2	4.8	7.9	0	–	–
Pt,Sn-1	Pt,Sn/Mg(Al)O	4.8	3.0	7.2	168	99
$PtSn_2$	$PtSn_2$ alloy	–	45.1	54.9	–	–

[a] The crystallite size (one side length) was calculated from the measured BET surface area assuming cubic particles.
[b] Not measured.

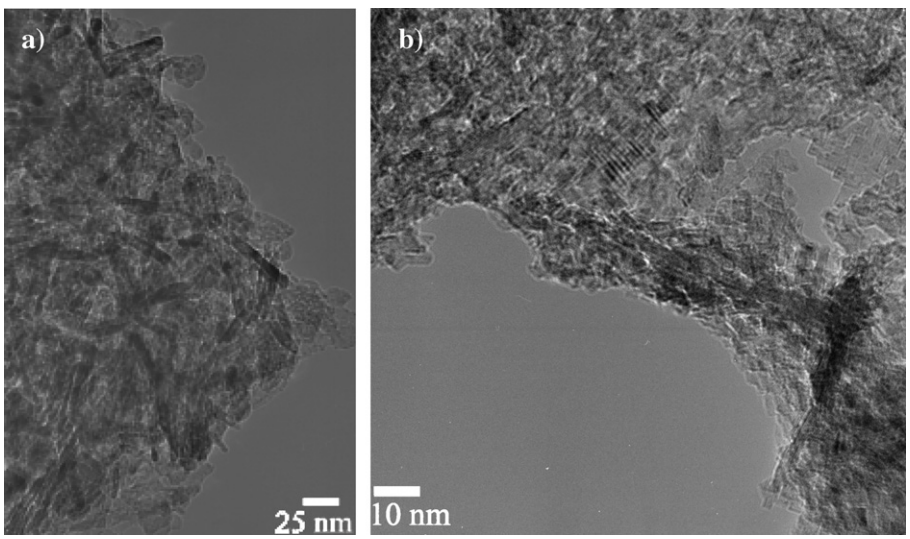

Fig. 1. TEM pictures of (a) Sample HT and (b) Sample Pt-2.

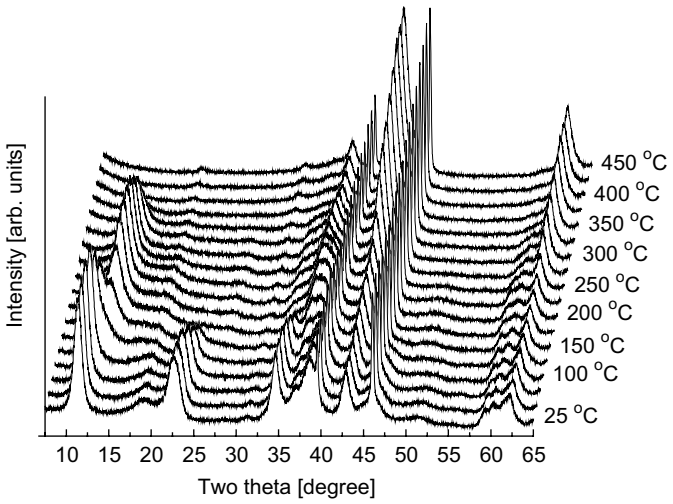

Fig. 2. Temperature resolved XRD-patterns of a Mg(Al)O sample after storage in air for several months, during heating to 450 °C in air. The reflexes at $2\theta = 39.5°$ and 46.0° are Pt reflexes from the Pt sample holder.

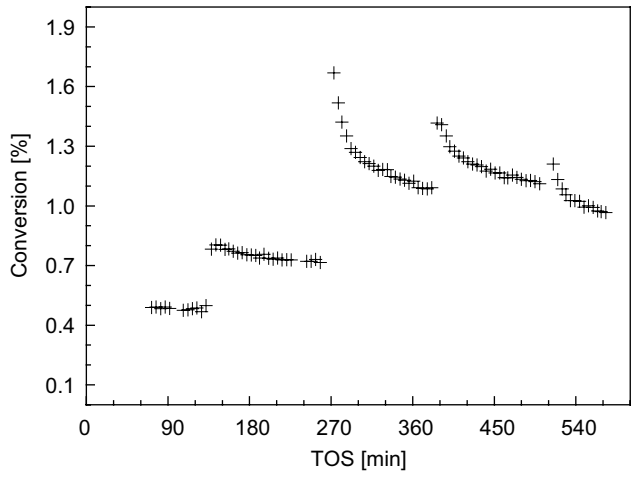

Fig. 3. Activation of sample Pt,Sn-1 in a conventional test reactor at 450 °C. Reaction conditions: H_2:C_2H_6:CO_2:Inert = 1:6.3:4.3:51, 450 °C, 1 atm, WHSV = 1.6 h^{-1}.

Catalytic activity data obtained during ethane dehydrogenation experiments over sample Pt,Sn-1 at 450 °C in a conventional reactor are shown in Fig. 3. In the catalytic tests, steam in the feed was exchanged with CO_2 for technical reasons. Earlier tests have shown that the activation pattern is similar for CO_2 and H_2O containing feeds. The results in Fig. 3 clearly show that sample Pt,Sn-1 has the same activity pattern as the low-metal loading analogue used in a previous study [15]; the initial dehydrogenation activity increases from the first to the second and third test-regeneration cycles, even at 450 °C (i.e., the *in situ* XPS measurement temperature).

MS data obtained for the effluent of the *in situ* XPS cell during three test cycles of Pt,Sn-1 are shown in Fig. 4. Characteristic masses of products ethene (*m*/*e* 28) and CO_2 (*m*/*e* 44) are shown relative to the molecular ion peak

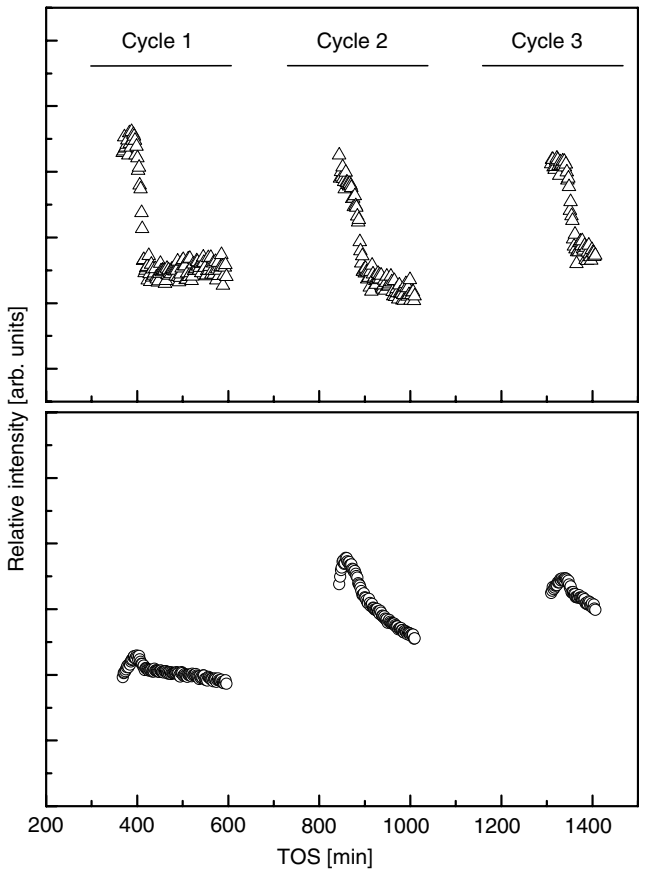

Fig. 4. Activation of sample Pt,Sn-1 during *in situ* XPS measurements under reaction conditions at 450 °C. H_2:C_2H_6:H_2O = 1:1.5:7.5, total pressure 0.3 mbar. Upper curve: [(*m*/*e* 28):(*m*/*e* 30)], representing ethene production. Lower curve: [(*m*/*e* 44):(*m*/*e* 30)], representing CO_2 production.

of ethane (*m*/*e* 30). The results in Fig. 4 clearly show that Pt,Sn-1 was active for ethane dehydrogenation as well as for oxidation by H_2O during the *in situ* XPS measurements. Similar results were obtained for $PtSn_2$ alloy and Pt-2, while no activity was observed over Pt-1.

3.2. XPS data

3.2.1. Depth profiling of Mg and Al. Samples HT, Pt-1 and Pt-2

Fig. 5 shows the Mg/Al or Mg/(Al + Pt) ratios as a function of the analysis depth (10–21 Å) in Samples HT, Pt-1 and Pt-2 under different atmospheres, all at 450 °C. There is no general trend in the Mg/Al(+Pt) ratios observed with increasing analysis depth, and the results presented in Fig. 5 suggest that Mg and Al are evenly distributed within the material depths covered by the analyses. The experimental error of the calculated ratio is set to 20% (as indicated by error bars for one data set), estimated from the background subtraction of the Mg and Al peaks. The large error in the calculated area ratio arises mostly from the uncertainty in background subtraction for the Al peak, due to inelastically scattered Mg-electrons in the

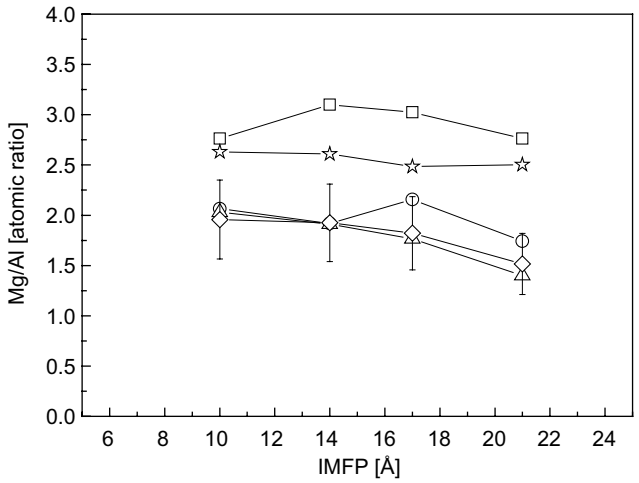

Fig. 5. Mg/Al or Mg/(Al + Pt) atomic ratio in the support material as function of analysis depth. □ Sample HT under reaction conditions, ☆ Sample Pt-1 under reaction conditions, ○ Sample Pt-2 under reaction conditions, △ Sample Pt-2 under oxidation conditions, ◊ Sample Pt-2 in hydrogen–water mixture, all at 450 °C (see Table 1 for details).

gas phase of the chamber, on top of which the Al peak resides.

From BET and TEM measurements presented in Fig. 1 and Table 4, the crystallite diameter of Mg(Al)O used in this study is estimated to 50–150 Å. Thus, the highest photon energy used, corresponding to an inelastic mean free path of 21 Å, covers half the radius of an average Mg(Al)O crystallite, and should be representative for the bulk composition of the crystallites. In conclusion, the results strongly suggest that Mg and Al are homogeneously distributed throughout the Mg(Al)O crystallites. It has previously been suggested in literature that the Mg(Al)O surface is enriched in Al [12–14]. It should be noted, however, that those results were based on a comparison between ICP analysis and XPS data obtained at constant photon energy, i.e., Al Kα radiation at 1487 eV [12]. Although XPS is a surface-sensitive technique, the data obtained in the present study may indicate that the previously reported deviation between XPS and ICP data are related to uncertainties in the theoretical photoionisation cross section of the XPS peaks, as previously reported for VPO catalysts [38,39].

Such deviation is observed also in the present study, where the Mg/Al ratio determined by XPS (1.3–3.2) is significantly lower than 4.8 determined by ICP analysis (Fig. 5 vs. Table 4). Samples HT and Pt-1 have significantly higher Mg/Al ratios compared to sample Pt-2. The reason for this could be the higher Pt content in sample Pt-2, which contributes to the Al-peak area, giving a lower Mg/Al ratio for this sample. Deconvolution of the Al + Pt peak (see below) and subtraction of the Pt area gave similar Mg/Al ratios to the HT sample (not shown).

Fig. 6 shows the Mg 2p peak fitted with a Gaussian curve as function of analysis depth in sample HT (Mg(Al)O) under reaction conditions at 450 °C. Due to differential charging of the sample during XPS measurements,

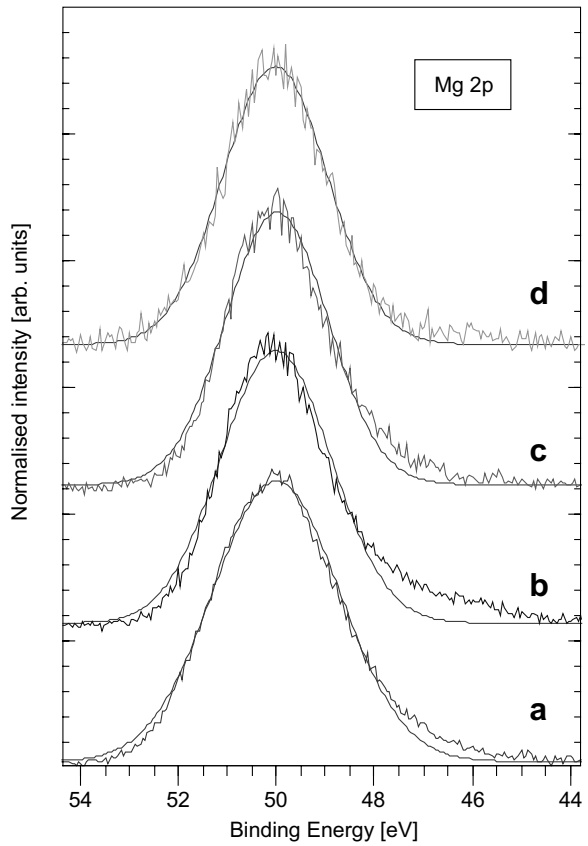

Fig. 6. The Mg 2p peak at analysis depth of (a) 10 Å, (b) 14 Å, (c) 17 Å and (d) 21 Å in calcined hydrotalcite (sample HT) under reaction mixture at 450 °C.

the position of the peak maximum has in each case been adjusted to an equal value of 50 eV for easier comparison of the peak shape. The peaks are symmetrical, indicating a constant binding energy (BE) with analysis depth; however, the FWHM is rather large (approximately 3 eV), and minor changes in BE would not be detectable. Fig. 7 shows the Mg 2p peak for samples HT, Pt-1 and Pt-2 at 10 Å analysis depth under reaction conditions, as well as sample Pt-2 under different gas atmospheres, all at 10 Å analysis depth. A Gaussian peak profile shape is also shown. A comparison of peak shapes shows the appearance of a slight asymmetry in the Pt-containing samples. Further, it is observed that the asymmetry varies slightly with gas composition for Pt-2. Pt, Al or O do not have binding energies in the 46–54 eV range, so the asymmetry cannot be due to overlap with XPS peaks of other elements. Further, Mg is very stable in the +2 oxidation state, and a shoulder towards lower binding energy under oxidative conditions is not likely. Another possible explanation for the peak broadening is overlap with Auger peaks. However, varying the photon energy (not shown) did not lead to changes in the peak broadening, and this explanation was therefore ruled out. In conclusion, the irregular Mg 2p peak shape of Pt-containing samples is probably due to differential charging of the samples.

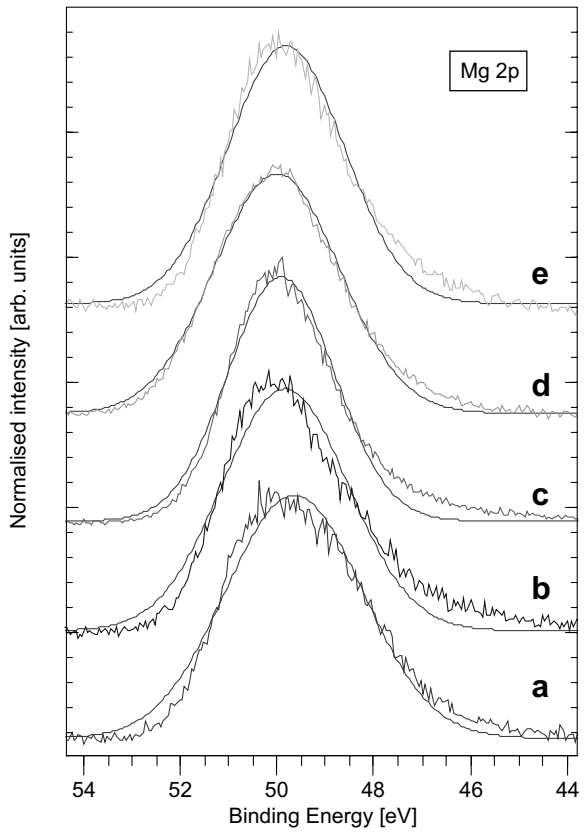

Fig. 7. The Mg2p peak in samples Pt-2, HT and Pt-1 at 10 Å analysis depth. (a) Pt-2 in reaction mixture, (b) Pt-2 in oxygen, (c) Pt-2 in hydrogen-steam mixture, (d) HT in reaction mixture, (e) Pt-1 in reaction mixture, all at 450 °C.

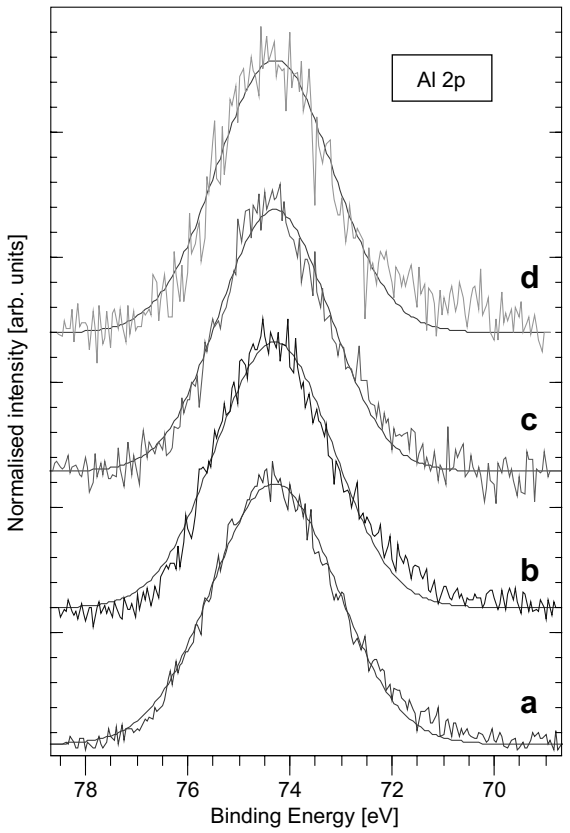

Fig. 8. Al2p peak at analysis depth of (a) 10 Å, (b) 14 Å, (c) 17 Å and (d) 21 Å in sample HT under reaction conditions.

Fig. 8 shows the Al2p peak observed for sample HT at different analysis depths under reaction conditions. As for the Mg2p peak, it is observed that the Al2p peak is symmetrical and similar at all analysis depths for sample HT. Figs. 9 and 10 show the Al2p peak together with the Pt4f doublet in sample Pt-2 under reaction conditions at different analysis depths, and in samples Pt-2 and Pt-1 in different gas compositions at 10 Å analysis depth. The experimental peaks are clearly not symmetrical, and peak deconvolution was carried out. The results shown are representative of all obtained results: When referenced to the Al2p peak at 74.3 eV, a typical binding energy of the Al^{3+} state in aluminium oxides [40,41], the binding energy of Pt $4f_{7/2}$ falls in the region 70.8–72.4 eV. These BE values indicate the presence of large amounts of reduced Pt under all conditions, in agreement with thermodynamic calculations (using thermodynamic data from Ref. [42]), which indicated that Pt is fully reduced even under oxidation in 0.3 mbar O_2 at 450 °C.

3.2.2. Sn/Mg ratio. Sample Pt,Sn-1

Sn/Mg atomic ratios measured during three subsequent ethane dehydrogenation test-regeneration cycles and at two analysis depths are shown in Fig. 11. The sample was moved twice during the measurement sequence, i.e., at 7.5 h and 21 h on-stream, because of differential charging of the sample. The homogeneity of the sample was tested at three areas after completing the sequence, and the measurements indicate that some inhomogeneity may occur (the highest measured Sn/Mg difference was 25% relative). This means that caution must be shown when comparing the Sn/Mg ratios obtained before and after moving the sample. With this in mind, three distinct features are apparent from Fig. 11: First, the Sn/Mg ratio is highest closer to the sample surface. This result indicates that tin is mainly located on the outer surface of the sample, as expected when using the impregnation technique. Second, the Sn/Mg ratio on the surface relative to the Sn/Mg ratio deeper into the sample does not change significantly (average value 1.8 ± 0.3) with time on stream (TOS). This observation indicates that tin does not diffuse into the material with time, but stays on the outer surface. Third, it is interesting to observe that the Sn/Mg ratio measured at each set of gas compositions increases with increasing TOS. Together, these observations indicate that tin is initially located in defined clusters on the sample surface. With time on stream, tin gradually spreads from the clusters, covering an increasing fraction of the Mg(Al)O surface. Thorough investigation of Fig. 11 reveals that for each test-regeneration cycle, an increase in the Sn/Mg ratio is observed from reduction to reaction conditions, while it is either quite stable or decreases between the other conditions. Since

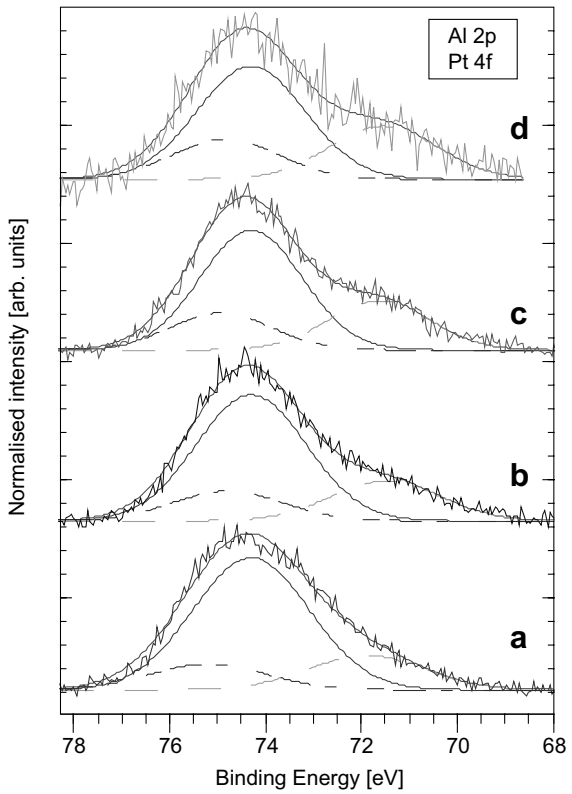

Fig. 9. Al2p peak together with Pt4f doublet in the sample Pt-2 under reaction conditions at analysis depth of (a) 10 Å, (b) 14 Å, (c) 17 Å and (d) 21 Å.

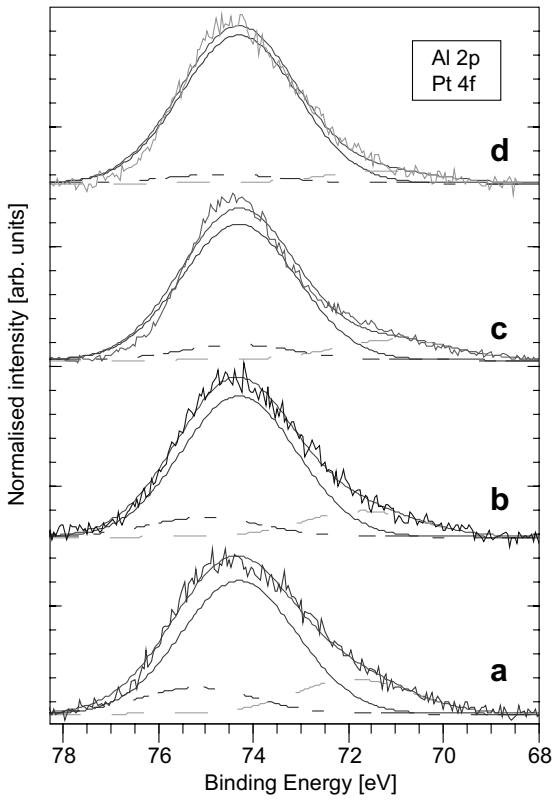

Fig. 10. Al2p peak together with Pt4f doublet in the samples Pt-2 and Pt-1 at 10 Å analysis depth. (a) Pt-2 in reaction mixture, (b) Pt-2 in oxygen, (c) Pt-2 in hydrogen-steam mixture and (d) Pt-1 in reaction mixture, all at 450 °C.

each measurement was performed soon after switching conditions, this observation suggests that spreading of tin takes place predominantly under reduction conditions.

Bednarova et al. have reported that the Pt content of Pt,Sn particles on Pt,Sn/Mg(Al)O and Pt,Sn/Al_2O_3 catalysts increased during reduction at 600 °C, based on TEM analysis [16]. In addition to confirming their findings, our results point to the placement of Sn at the outer surface of the carrier material after diffusion from the Pt,Sn particles, and to the diffusion proceeding predominantly during reduction treatment. It has previously been reported that tin may be present on the support surface in Pt,Sn/Al_2O_3 [43,44] and Pt,Sn/ZrO_2 catalysts [17].

The Sn 3d doublet scanned at two analysis depths and in different gas mixtures is shown in Fig. 12. There is no sign of asymmetry of the Sn peaks, and the peaks can be fitted well with one Gaussian curve. Because of similar chemical shifts of the Sn^{2+} and Sn^{4+} peaks, it is not possible to distinguish between these two oxidation states of tin by examining the shape of the peaks [45]. However, it would be possible to see changes in the peak shape if the oxidation state of Sn would change between $Sn^{2+/4+}$ and Sn^0, as the chemical shift of Sn 3d in tin oxides compared to pure tin is usually reported to be in the region of 1.5–1.8 eV [45–47]. An even larger separation between oxidised and metallic tin has been observed in supported Pt–Sn catalysts. De Miguel et al. [48] observed a separation of approximately 3 eV in alumina and K-doped alumina supported catalysts, and a separation of 2.3 eV in Pt,Sn/MgO.

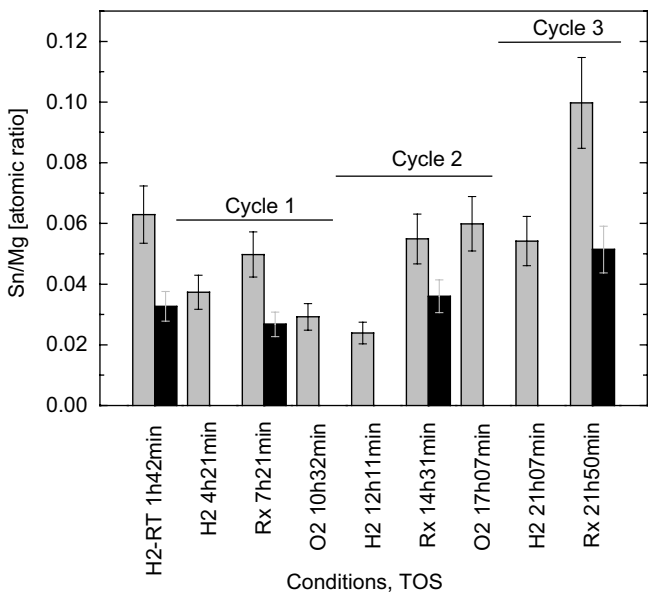

Fig. 11. Sn/Mg atomic ratio in sample Pt,Sn-1 at 10 Å (grey bars) and 14 Å (black bars) analysis depth.

Several ESCA studies performed on Pt–Sn catalysts supported on alumina have observations similar to ours, that

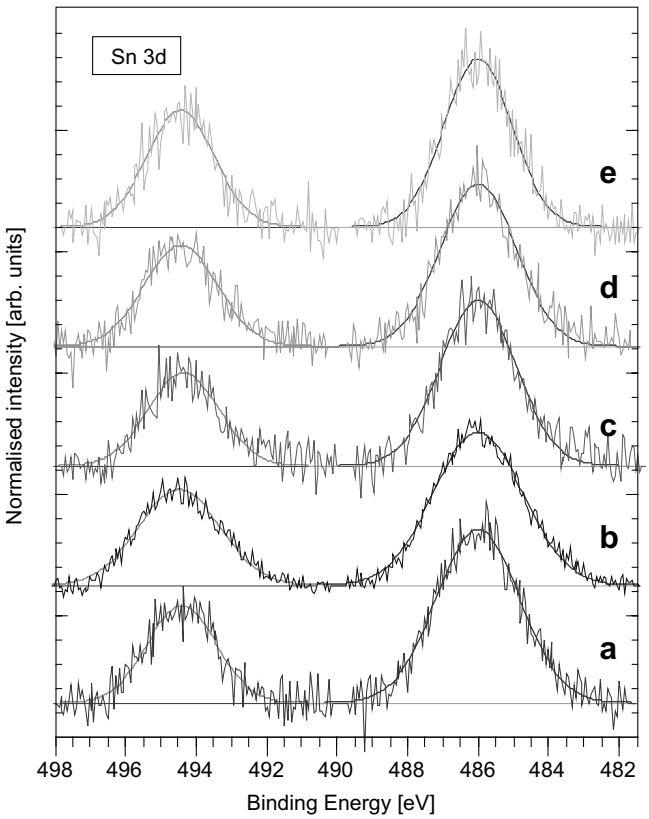

Fig. 12. Sn 3d doublet in sample Pt,Sn-1 at two analysis depths and in different gas mixtures, (a) 10 Å, H_2, room temperature, (b) 10 Å, O_2, 450 °C, (c) 10 Å, H_2 450 °C, (d) 10 Å, reaction mixture, 450 °C and (e) 14 Å, reaction mixture 450 °C.

the shape of Sn 3d doublet indicates the presence of one oxidation state only. Because of easier referencing in ESCA technique, from the binding energy of the Sn $3d_{5/2}$ peak these studies conclude that the lowest oxidation state of tin present on alumina is Sn^{2+} [46,47,49]. Our observations of Sn supported on mixed oxide correlate well with the mentioned observations of Sn supported on alumina, as no change in the oxidation state of Sn is visible. These observations may suggest that within the spectral resolution, Sn on the catalyst surface is in an oxidised state under all conditions. This conclusion is further supported by the measurements performed on the $PtSn_2$ alloy, presented below. It should be noted that, although the Sn 3d doublet of Pt,Sn/Mg(Al)O is symmetrical and can be fitted with one Gaussian curve, a second component with low but not zero intensity could be present, without introducing visual changes in the shape of the overall peak. With an average FWHM of the Sn $3d_{5/2}$ peak of 2.6 eV and an average separation of 1.7 eV between the peaks of $Sn^{2+/4+}$ and Sn^0 states, we estimate the intensity of a possible second component to be within 15% of the overall peak intensity, as also estimated by Adkins and Davis in [49].

The Mg/(Al + Pt) ratio of sample Pt,Sn-1 was measured at two analysis depths during the same activation sequence, and is shown in Fig. 13. The Mg/(Al + Pt) ratio decreases slightly with time on stream, suggesting that the Pt distribution is unchanged or increases slightly throughout the sequence. This result is in disagreement with results reported previously based on TEM analysis, that Pt sinters during testing of a Pt,Sn/Mg(Al)O catalyst [16]. A possible reason for the discrepancy is the higher temperature used in their case (600 vs. 450 °C), as well as the low visibility of small Pt particles in TEM [16].

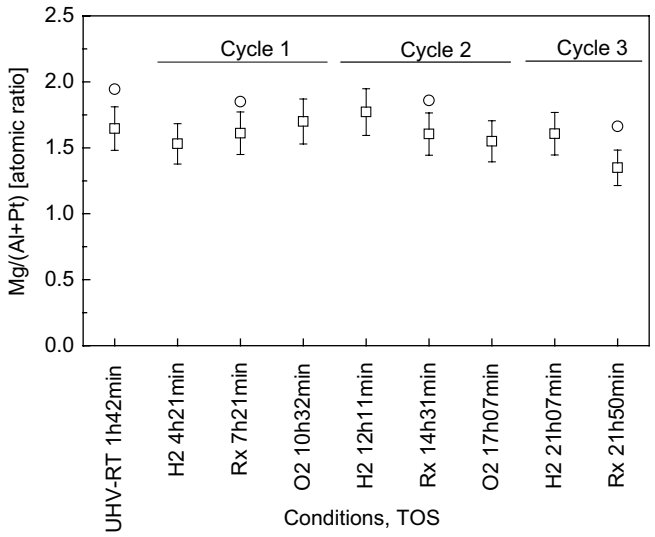

Fig. 13. Mg/(Al + Pt) atomic ratio in sample Pt,Sn-1 at 10 Å (□) and 14 Å (○) analysis depth.

The uncertainty from the background subtraction is in this case estimated to be 10%. The reason for the lower uncertainty compared to the HT and Pt-1 and Pt-2 samples is better quality of the detail-scans with wider regions in many cases, which makes it easier to subtract an equal background.

3.2.3. Pt/Sn ratio and oxidation state. $PtSn_2$ alloy

Fig. 14 shows the Pt/Sn ratio in $PtSn_2$ alloy at two analysis depths as a function of analysis conditions and time on stream. Two distinct features are apparent: First, the Pt/Sn ratio decreases upon heating from room temperature to 450 °C and upon switching from H_2 to reaction mixture at 450 °C. Second, a higher Pt/Sn ratio is observed at greater depth under reduction and reaction conditions. The result is in agreement with previous literature reports, which concluded that the surface of Pt–Sn alloys and supported Pt–Sn particles is enriched in Sn after reduction at 500–600 °C, probably due to the lower surface energy of Sn compared to Pt [43,50,51]. Bouwman et al. [50] further reported that the oxidation of the annealed surface of the PtSn and Pt_3Sn alloys caused a further enrichment of the surface with Sn. This observation indicates that Sn diffuses towards the surface of the alloy under all tested conditions.

For $PtSn_2$ alloy the differential charging problem was avoided, and the binding energies of Pt and Sn could be measured during use. The position of the Sn 3d and 4d peaks was calibrated from the corresponding Fermi edge

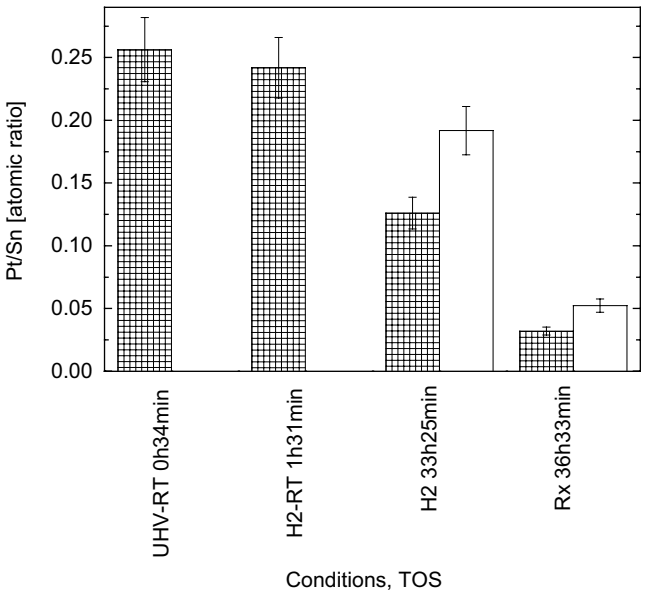

Fig. 14. Pt/Sn atomic ratio in $PtSn_2$ alloy under different conditions (see Table 1 for details) and at two analysis depths: 8 Å (squared bars) and 15 Å (white bars).

spectra. The detailed peak analysis procedure is described in Section 2.

Area ratios resulting from curve fitting of Sn 3d and Sn 4d peaks are shown in Table 5. The deconvolution of the peaks into two oxidation states is shown in Figs. 15–17. The binding energies of the two Sn 3d components observed are 485.3 and 486.6 eV. The binding energy of the 3d peak of oxidised tin (Sn^{2+} and Sn^{4+}) in tin oxides is usually reported in the region 486–487 eV [40,45,49]. The component with the binding energy of 486.6 eV can therefore be characterised as tin present as tin oxide. The component at 485.3 eV has a slightly higher binding energy than Sn 3d in metallic state, which has a binding energy of 484.9 eV [35,36,52]. In a study of oxidation of ordered Pt–Sn surface alloys Jerdev and Koel [52] attributed a peak at a BE of 485.5 eV to "quasimetallic" Sn, a state resembling O–Sn chemisorption state. Bouwman and Biloen [53] observed a Sn $3d_{5/2}$ binding energy of 485.5 eV in reduced PtSn alloy, close to the low binding energy component observed in our work.

The Sn 4d peak was also resolved to two oxidation states with average binding energies for $4d_{5/2}$ of 25.9 and 24.5 eV.

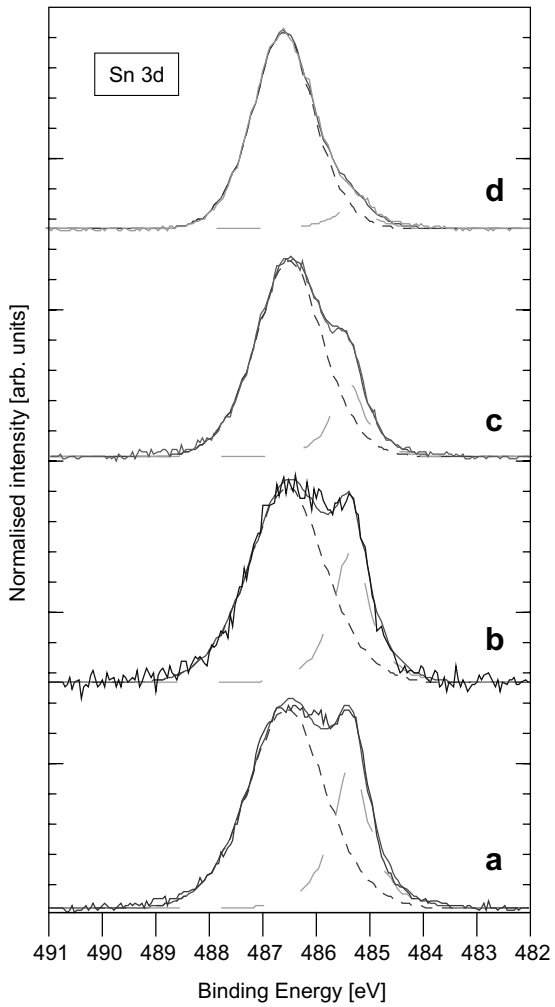

Fig. 15. Deconvolution of Sn 3d peak in $PtSn_2$ alloy at 8 Å analysis depth under following conditions: (a) in UHV at RT, (b) in H_2 at RT, (c) in H_2 at 450 °C and (d) in reaction mixture at 450 °C.

This corresponds well with the oxidation states found from the deconvolution of the Sn 3d peak, since Sn 4d of metallic tin has a binding energy of 23.9 eV [35,36]. In conclusion, the results obtained in this study indicate that Sn is predominantly in an oxidised state (Sn^{2+} or Sn^{4+}) at the surface of Pt–Sn particles, while the remainder of Sn in the outer layers is alloyed with Pt.

In addition to showing that the major part of Sn on the surface of the $PtSn_2$ alloy is in an oxidised state under all

Table 5
Area ratios of different oxidation states of Sn in $PtSn_2$ alloy

Gas mixture	T [°C]	Area %, Sn 3d, 8 Å		Area %, Sn 4d, 8 Å		Area %, Sn 4d, 15 Å	
		Oxidised BE 486.6 eV	Alloyed BE 485.3 eV	Oxidised BE 25.8–26.0 eV	Alloyed BE 24.3–24.7 eV	Oxidised BE 25.8–26.0 eV	Alloyed BE 24.3–24.7 eV
UHV	Ambient	72	28	83	17	–[a]	–
H_2	Ambient	73	27	84	16	–	–
H_2	450	83	17	83	17	65	35
H_2O:H_2:C_2H_6	450	93	7	98	2	93	7

[a] Not measured.

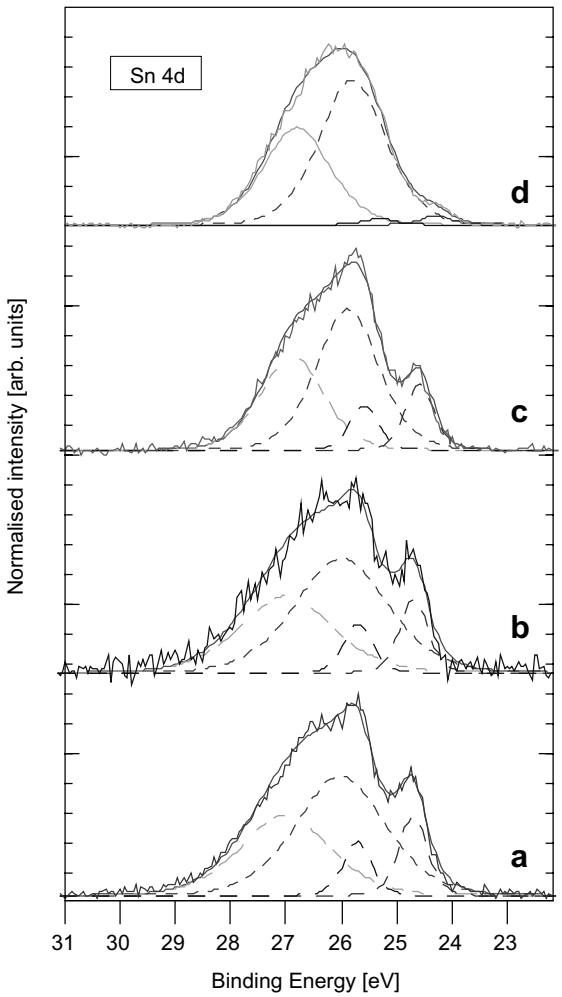

Fig. 16. Deconvolution of Sn 4d peak in $PtSn_2$ alloy at 8 Å analysis depth under following conditions: (a) in UHV at RT, (b) in H_2 at RT, (c) in H_2 at 450 °C and (d) in reaction mixture at 450 °C.

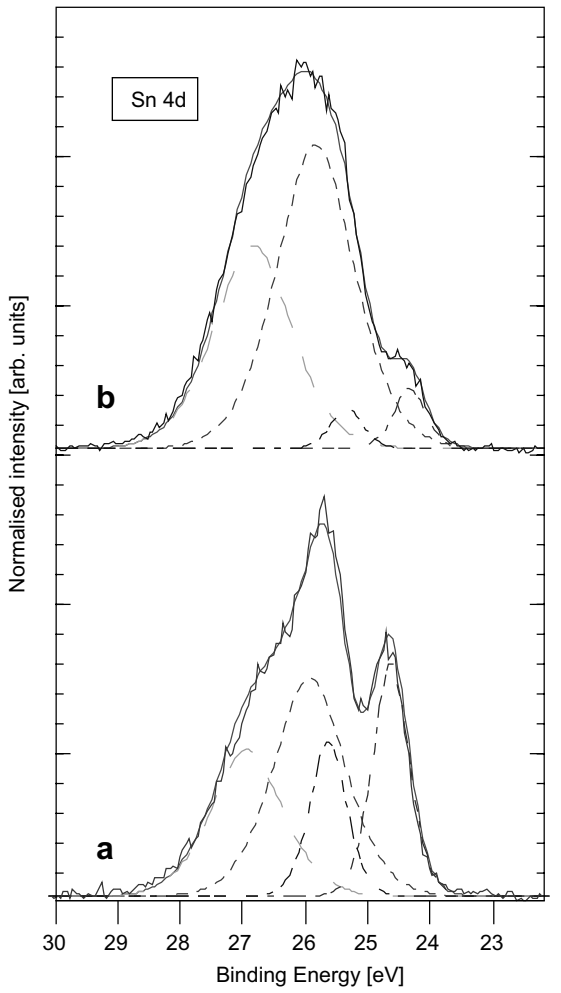

Fig. 17. Deconvolution of Sn 4d peak in $PtSn_2$ alloy at 15 Å analysis depth under following conditions: (a) in H_2 at 450 °C and (b) in reaction mixture at 450 °C.

tested conditions, the data in Table 5 and Figs. 15–17 indicate that under reduction conditions, the amount of alloyed Sn is higher at 15 Å analysis depth than at 8 Å analysis depth. When going from reduction to reaction conditions, the amount of reduced Sn decreases to below 10% at both analysis depths.

The shape and positions of Pt 4f peaks measured at 15 Å analysis depth did not change when switching from hydrogen to reaction mixture within the experimental error (which is in this case estimated to ±0.2 eV from the FE calibration). The BE of the Pt 4f peak at 15 Å is 72.0 eV. This binding energy is somewhat higher than reported for Pt $4f_{7/2}$ in metallic Pt (71.2 eV) [35]. A Pt $4f_{7/2}$ binding energy in reduced PtSn alloy of 72.0 eV is reported in [53], who further reported a BE of 71.8 eV for Pt $4f_{7/2}$ in reduced, metallic Pt. It has been observed previously that tin induces a shift of the Pt $4f_{7/2}$ core level to higher BE compared to pure Pt [54]. A shift of the Pt 4f peak to higher BE has also been reported in Co–Pt alloys [55] and upon addition of Sn to Ni–Nb–Sn–Pt alloys [56]. The shape of Pt 4f peaks at 8 Å analysis depth is the same as for the peaks at 15 Å analysis depth. It is also unchanged under all conditions, except for a decrease in peak width when heating the sample. Because of a feature rich FE at 390 eV photon energy, the energy calibration was more uncertain for these peaks, but the same BE as for the 15 Å peaks is indicated (approximately 71.7 ± 0.4 eV). In conclusion, the results obtained in our study indicate that Pt close to the sample surface is alloyed with Sn.

The results observed for the $PtSn_2$ alloy are in agreement with thermodynamic calculations (using thermodynamic data from Ref. [42]), which indicated that Pt is fully reduced even under reaction and oxidation conditions at 450 °C, while Sn is oxidised (preferably as Sn^{4+}) under reaction conditions, and SnO_2 even has a positive Gibbs energy of reduction in a H_2 atmosphere, at 450 °C. On the other hand, the reaction:

$$SnO_2 + Sn = 2SnO$$

has a Gibbs free energy of +6 kJ/mol at 450 °C, and is not favourable. This result indicates that Sn which migrates to the particle surface under reduction conditions at 450 °C

will remain in a reduced state. While $PtSn_2$ alloy has a melting point of 745 °C, Sn^0 melts already at 232 °C; well below the temperature of reduction and reaction (450 °C) [57]. The presence of highly mobile, melted Sn^0 near the particle surface under reduction conditions could explain why Sn in sample Pt,Sn-1 preferably migrates from the metal particles to the support surface during reduction (cf. Fig. 11).

The presence of Pt could influence the red-ox behaviour of Sn. Safonova et al. recently studied reduction of SnO_2 thin films with or without metal dopage ($M = Pt, Pd, Cu, Ni$) in $1\%H_2/N_2$ mixtures. Pt and Pd showed similar effects, but only the Pd-doped system was studied in detail. Only a minor shift (<0.15 eV) in the Sn $3d_{5/2}$ peak of the XPS spectrum was observed after annealing Pd-doped SnO_2 in $1\%H_2/N_2$ at 380 °C for 4 h compared to the same treatment in O_2 [58], in line with our results.

3.3. Influence on catalytic properties

The catalytic test results in Fig. 3 show two effects of repeated test-regeneration cycles: The initial activity after regeneration increases, while the stability within one test cycle decreases. The results in Fig. 11 indicate that Sn migrates to the support surface during reduction between the test cycles. This result suggests that the initial activity increase observed from cycle 1 to cycle 3 is related to an increased Pt concentration at the metal particle surface, due to migration of Sn to the support surface. Deactivation within each test cycle could either be due to coke formation or to metal particle sintering. The results in Fig. 13 which indicate that Pt dispersion is stable with time on stream, strongly suggest that particle sintering is not responsible for the observed deactivation within test cycles 1–3. The increasing deactivation rate within each test cycle with TOS can therefore be correlated to a change in catalyst selectivity from ethene to carbon deposits. *In situ* XPS measurements of the C 1s peak performed during activation treatment did not reveal carbon deposits on the catalyst surface after first oxidation. The only carbon peaks visible were due to CO_2 and ethane/ethene present in the gas phase under reaction conditions. It is well documented in literature that Sn promotion of Pt catalysts leads to less carbon deposition (see e.g. [17,21,24]); however, there is controversy about the reason for this selectivity change. Stagg et al. recently suggested that a basic support material, such as ZrO_2, may contribute to the stability of Pt,Sn catalysts by providing oxygen to the metal, thereby promoting oxidation of coke deposits. Migration of Sn from Pt,Sn metal particles would lead to coverage of the basic sites on the ZrO_2 surface, thereby reducing the stability of the catalyst [17]. Other groups have suggested that a change in the electronic properties of the Pt metal [22,59,60], or in the Pt cluster size [60], or even unmasking of specific sites [61], may contribute to a change in the reaction selectivity of metal catalysts. However, we are presently not in position to distinguish between these alternative explanations for the catalyst under study.

4. Conclusion

The results obtained in the present study contribute to a detailed understanding of the Pt,Sn/Mg(Al)O catalyst system, which has shown excellent properties as a light alkane dehydrogenation catalyst. We have performed *in situ* XPS measurements of Pt(Sn)/Mg(Al)O catalysts under constant gas flow and at temperatures close to those used in ethane dehydrogenation. Our measurements indicate that Al and Mg are evenly distributed in the crystallites of the mixed oxide used as carrier material. In Pt/Mg(Al)O catalysts, reduced Pt is present under all conditions. A Pt,Sn/Mg(Al)O catalyst was studied throughout several test-regeneration cycles. The measurements indicate that tin is initially located in defined clusters on the sample surface. During activation treatment (predominantly under reduction conditions), tin gradually spreads from the clusters, covering an increasing fraction of the Mg(Al)O surface. The majority of Sn is present in an oxidised state under all conditions. A $PtSn_2$ alloy was studied separately. The $PtSn_2$ alloy showed surface enrichment in Sn under reduction and reaction conditions. The majority of Sn on the surface of the $PtSn_2$ alloy is in an oxidised state under all conditions, while the remainder is alloyed with Pt. Pt is present in the reduced state alloyed with Sn under all conditions.

Acknowledgements

A.V.'s Ph.D. grant is financed by Statoil through the VISTA programme, contract no. 6446. Travel funding for A.V.'s stay at BESSY was obtained through the Norwegian-German Project Based Personnel Exchange Programme at the Norwegian Research Council. Ole Bjørn Karlsen (UiO) and Aud I. Spjelkavik (SINTEF) are gratefully acknowledged for the preparation of catalyst samples used in this study. The BESSY staff is acknowledged for technical support during the *in situ* XPS measurements.

References

[1] J.A. Moulijn, M. Makkee, A. van Diepen, Chemical Process Technology, John Wiley & Sons, Chichester, 2001.
[2] E. Rytter, U. Olsbye, P. Soraker, R. Torvik, WO Patent 2001055062 A1 20010802, 2001, to Den Norske Stats Oljeselskap AS.
[3] C.L. Thomas, Catalytic Processes and Proven Catalysts, Academic Press, New York, 1970.
[4] L. Bednarova, Study of supported Pt–Sn catalysts for propane dehydrogenation, Ph.D. Thesis, Norwegian University of Science and Technology (NTNU), 2002, p. 47.
[5] F. Cavani, F. Trifiro, A. Vaccari, Catal. Today 11 (1991) 173.
[6] M. Bellotto, B. Rebours, O. Clause, J. Lynch, J. Phys. Chem. 100 (1996) 8535.
[7] D. Akporiaye, M. Roennekleiv, P. Hasselgaard, NO Patent 308989, 2000, to Den Norske Stats Oljeselskap AS.
[8] D. Tichit, B. Coq, Cattech 7 (2003) 206.
[9] T. Shishido, M. Sukenobu, H. Morioka, R. Furukawa, H. Shirahase, K. Takehira, Catal. Lett. 73 (2001) 21.
[10] A. Olafsen, A. Slagtern, I.M. Dahl, U. Olsbye, Y. Schuurman, C. Mirodatos, J. Catal. 221 (2005) 163.

[11] U. Olsbye, D. Akporiaye, E. Rytter, M. Ronnekleiv, E. Tangstad, Appl. Catal. A 224 (2002) 39.
[12] A.L. McKenzie, C.T. Fishel, R.J. Davis, J. Catal. 138 (1992) 547.
[13] J.I. Di Cosimo, V.K. Diez, M. Xu, E. Iglesia, C.R. Apesteguia, J. Catal. 178 (1998) 499.
[14] D. Jiang, B. Zhao, Y. Xie, G. Pan, G. Ran, E. Min, Appl. Catal. A 219 (2001) 69.
[15] D. Akporiaye, S.F. Jensen, U. Olsbye, F. Rohr, E. Rytter, M. Ronnekleiv, A.I. Spjelkavik, Ind. Eng. Chem. Res. 40 (2001) 4741.
[16] L. Bednarova, C.E. Lyman, E. Rytter, A. Holmen, J. Catal. 211 (2002) 335.
[17] S.M. Stagg, E. Romeo, C. Padro, D.E. Resasco, J. Catal. 178 (1998) 137.
[18] R.D. Cortright, J.M. Hill, J.A. Dumesic, Catal. Today 55 (2000) 213.
[19] J. Llorca, N. Homs, J. Leon, J. Sales, J.L.G. Fierro, P. Ramirez de la Piscina, Appl. Catal. A 189 (1999) 77.
[20] M.M. Schubert, M.J. Kahlich, G. Feldmeyer, M. Huttner, S. Hackenberg, H.A. Gasteiger, R.J. Behm, PCCP 3 (2001) 1123.
[21] Z. Tian, Y. Xu, L. Lin, Chem. Eng. Sci. 59 (2004) 1745.
[22] J. Jia, L. Lin, J. Shen, Z. Xu, T. Zhang, D. Liang, Y. Chen, Sci. China B 41 (1998) 606.
[23] G. Aguilar-Rios, M. Valenzuela, P. Salas, H. Armendariz, P. Bosch, G. Del Toro, R. Silva, V. Bertin, S. Castillo, A. Ramirez-Solis, I. Schifter, Appl. Catal. A 127 (1995) 65.
[24] O.A. Barias, Transient kinetic investigation of the catalytic dehydrogenation of propane, Ph.D. Thesis, Norwegian University of Science and Technology (NTH), 1993, p. 104.
[25] H. Armendariz, A. Guzman, J.A. Toledo, M.E. Llanos, A. Vazquez, G. Aguilar-Rios, Appl. Catal. A 211 (2001) 69.
[26] Z. Li, M.S.J. Tu, J. Jia, Z. Xu, L. Lin, Cuihua Xuebao 19 (1998) 1.
[27] J. Hafizovic, Mekanismestudie av platinaavsetning på hydrotalcitt med ulike karakteriseringsmetoder, M.Sc. Thesis, University of Oslo, 04/2004.
[28] M.R. Weiss, R. Follath, K.J.S. Sawhney, F. Senf, J. Bahrdt, W. Frentrup, A. Gaupp, S. Sasaki, M. Scheer, H.C. Mertins, D. Abramsohn, F. Schafers, W. Kuch, W. Mahler, Nucl. Instrum. Meth. A 467-468 (2001) 449.
[29] Phoibos 150 hemispherical analyzer, manufactured by Specs GmbH, Berlin.
[30] D.F. Ogletree, H. Bluhm, G. Lebedev, C.S. Fadley, Z. Hussain, M. Salmeron, Rev. Sci. Instrum. 73 (2002) 3872.
[31] NIST Electron Inelastic-Mean-Free-Path Database, Vers. 1.1.
[32] A. Akkerman, T. Boutboul, A. Breskin, R. Chechik, A. Gibrekhterman, Y. Lifshitz, Phys. Status Solidi B 198 (1996) 769.
[33] S. Tanuma, C.J. Powell, D.R. Penn, Surf. Interface Anal. 21 (1994) 165.
[34] R.A. Pollak, S. Kowalczyk, L. Ley, D.A. Shirley, Phys. Rev. Lett. 29 (1972) 274.
[35] A. Thompson, D. Attwood, E. Gullikson, M. Howells, K. Kim, J. Kirz, J. Kortright, I. Lindau, P. Pianetta, A. Robinson, J. Scofield, J. Underwood, D. Vaughan, G. Williams, X-ray Data Booklet, Center for X-ray Optics and Advanced Light Source, Berkley, 2001.
[36] R. Nyholm, N. Martensson, J. Phys. C 13 (1980) L279.
[37] J. Rocha, M. del Arco, V. Rives, M.A. Ulibarri, J. Mater. Chem. 9 (1999) 2499.
[38] G.W. Coulston, E.A. Thompson, N. Herron, J. Catal. 163 (1996) 122.
[39] E. Kleimenov, H. Bluhm, M. Haevecker, A. Knop-Gericke, A. Pestryakov, D. Teschner, J.A. Lopez-Sanchez, J.K. Bartley, G.J. Hutchings, R. Schloegl, Surf. Sci. 575 (2005) 181.
[40] J.F. Moulder, W.F. Stickle, P.E. Sobol, K.D. Bomben, in: J. Chastain (Ed.), Handbook of X-ray Photoelectron Spectroscopy, Perkin–Elmer Corporation, Eden Prairie, 1992.
[41] O. Bose, E. Kemnitz, A. Lippitz, W.E.S. Unger, Fresenius J. Anal. Chem. 358 (1997) 175.
[42] I. Barin, O. Knacke, Thermodynamical Properties of Inorganic Substances, Springer-Verlag, Berlin, 1973.
[43] E. Merlen, P. Beccat, J.C. Bertolini, P. Delichere, N. Zanier, B. Didillon, J. Catal. 159 (1996) 178.
[44] J. Schwank, K. Balakrishnan, A. Sachdev, Stud. Surf. Sci. Catal. 75 (1993) 905.
[45] C.L. Lau, G.K. Wertheim, J. Vac. Sci. Technol. 15 (1978) 622.
[46] B.A. Sexton, A.E. Hughes, K. Foger, J. Catal. 88 (1984) 466.
[47] K. Balakrishnan, J. Schwank, J. Catal. 127 (1991) 287.
[48] S. De Miguel, A. Castro, O. Scelze, J.L. Garcia Fierro, J. Soria, Catal. Lett. 36 (1996) 201.
[49] S.R. Adkins, B.H. Davis, J. Catal. 89 (1984) 371.
[50] R. Bouwman, L.H. Toneman, A.A. Holscher, Surf. Sci. 35 (1973) 8.
[51] R. Bouwman, P. Biloen, Surf. Sci. 40 (1974) 348.
[52] D.I. Jerdev, B.E. Koel, Surf. Sci. 492 (2001) 106.
[53] R. Bouwman, P. Biloen, Anal. Chem. 46 (1974) 136.
[54] E. Janin, M. Bjoerkqvist, T.M. Grehk, M. Goethelid, C.M. Pradier, U.O. Karlsson, A. Rosengren, Appl. Surf. Sci. 99 (1996) 371.
[55] Y.-S. Lee, K.-Y. Lim, Y.-D. Chung, C.-N. Whang, Y. Jeon, Surf. Interface Anal. 30 (2000) 475.
[56] A. Kawashima, K. Asami, K. Hashimoto, Mater. Sci. Eng. A 134 (1991) 1070.
[57] T.B. Massalski, H. Okamoto, P.R. Subramanian, L. Kacprzak (Eds.), Binary Alloy Phase Diagrams, ASM International, Ohio, 1990.
[58] O.V. Safonova, M.N. Rumyantseva, R.I. Kozlov, M. Labeau, G. Delabouglise, L.I. Ryabova, A.M. Gaskov, Mater. Sci. Eng. B 77 (2000) 159.
[59] S.N. Coman, V.I. Parvulescu, M. De Bruyn, D.E. De Vos, P.A. Jacobs, J. Catal. 206 (2002) 218.
[60] S.R. De Miguel, M.C. Roman-Martinez, E.L. Jablonski, J.L.G. Fierro, D. Cazorla-Amoros, O.A. Scelza, J. Catal. 184 (1999) 514.
[61] R.T. Vang, K. Honkala, S. Dahl, E.K. Vestergaard, J. Schnadt, E. Laegsgaard, B.S. Clausen, J.K. Norskov, F. Besenbacher, Nat. Mater. 4 (2005) 160.
[62] D. Briggs, M.P. Seah (Eds.), Practical Surface Analysis, vol. 1, John Wiley & Sons, Chichester, 1990.